

# Machine learning-based Alpine treeline ecotone detection on ~~in~~ Xue Mountain ~~in~~ Taiwan

Geng-Gui Wang<sup>1</sup>, Min-Chun Liao<sup>2</sup>, Wei Wang<sup>3</sup>, Hui Ping Tsai<sup>1,4,\*</sup>, Hsy-Yu Tzeng<sup>5</sup>

5 <sup>1</sup>Department of Civil Engineering, and Innovation and Development Center of Sustainable Agriculture, National Chung Hsing University, Taichung City 402, Taiwan (R.O.C.)

<sup>2</sup> Chiayi Research Center, Taiwan Forestry Research Institute, Chiayi City 600, Taiwan (R.O.C.)

<sup>3</sup> Experimental Forest, National Chung Hsing University, No. 145 Xingda Rd., Taichung City 402, Taiwan (R.O.C.)

<sup>4</sup> i-Center for Advanced Science and Technology, National Chung Hsing University, Taichung City 402, Taiwan (R.O.C.)

10 <sup>5</sup> Department of Forestry, National Chung Hsing University, Taichung City 402, Taiwan (R.O.C.)

Correspondence to: Hui-Ping Tsai (email)

**Abstract.** Taiwan is characterized by high mountains density, with over 200 peaks exceeding 3,000 meters in elevation. The alpine treeline ecotone (ATE) Taiwan has the highest density of high mountains globally, with over 200 peaks exceeding 3,000 meters in elevation. The Alpine Treeline Ecotone (ATE) is a transitional zone between different vegetation types. The species distribution, range variations, and movement patterns of vegetation within the ATE are crucial indicators for assessing the impact of climate change and warming on alpine ecosystems. Therefore, this study focuses on the Xue Mountain glacial cirques in Taiwan (approximately 4 km<sup>2</sup>) and utilizes WorldView-2 satellite images from 2012 and 2021 to compute various vegetation indices and texture features (GLCM). By integrating these features with the Random Forest (RF) and U-Net models, we developed a classification map of the ATE in Xue Mountain. We analyzed changes in bare land, forest, krummholz, and shadows within the ATE from 2012 to 2021. The results indicate that the classification accuracy reached an overall accuracy (OA) of 0.838 when incorporating raw spectral bands along with vegetation indices and texture features (GLCM) (77 features in total). Feature importance ranking and selection reduced training time by 14.3% while ensuring alignment between field survey treeline positions and classification results. From 2012 to 2021, tree cover density increased, with the total forest area expanding by approximately 0.101 km<sup>2</sup>. The elevation of tree distribution rose by 32.00 ± 4.00 m, with the most significant area changes occurring between 3,500 and 3,600 m, while the 3,700 to 3,800 m range remained relatively stable. This study integrates remote sensing imagery with deep learning classification methods to establish a large-scale alpine treeline ecotone (ATE) classification map. The findings provide a valuable reference for the sustainable management of alpine ecosystems in the Xue Mountain glacial cirques in Taiwan.

## 1 Introduction

Taiwan is located in the subtropical region of Southeast Asia, with an elevation range of nearly 4,000 m, fostering diverse ecosystem types and rich biodiversity (Lin et al., 2021). The island contains more than 200 mountains exceeding 3,000 meters in elevation (Kuo et al., 2022), making it the highest-density alpine island in the world. Alpine zone ecosystems are particularly

35 vulnerable to environmental change due to their high environmental heterogeneity and limited species migration distances, especially when compared to broader latitudinal climate gradients and more resilient lowland regions ~~Alpine zone eesystems are susceptible to environmental changes compared to other regions~~ (Engler et al., 2011; Huss et al., 2017; Li et al., 2018; Zheng et al., 2020). The transition zone between trees and treeless vegetation in alpine ecosystems is known as the alpine treeline or the Alpine Treeline Ecotone (ATE) (Körner 2012). The ecological processes and changes in this zone are considered  
40 indicators of climate change (Chen et al., 2022), reflecting the interactions of climate, topography, species composition, and disturbance history (Loranger et al., 2016; Johnson et al., 2017; Mohapatra et al., 2019; Bader et al., 2021). Based on many studies, changes in the alpine treeline ecotone (ATE) illustrate the impacts of climate change on mountain ecosystems, such as the upward migration of tree species and increased tree density. However, these shifts are also influenced by other drivers, including land-use history, altered disturbance regimes (e.g., fire disturbance), herbivory pressure, and species-specific  
45 physiological traits ~~Furthermore, ATE changes illustrate the impact of climate change on the environment, such as the upward migration of tree species and an increase in tree density~~ (Wang et al., 2016; Johnson et al., 2017; Du et al., 2018; Mohapatra et al., 2019).

Recent advancements in remote sensing technology have empowered extensive studies on alpine treelines using various imagery sources with diverse spatial resolutions (Garbarino et al., 2023). Xu et al. (2020) utilized Landsat satellite imagery (30 m resolution) from 1987 to 2018 for Wuyishan National Park, China to examine the relationship between treeline position and climate based on the local indicator of spatial autocorrelation (LISA). They found that for every 1°C increase in temperature from 1987 to 2018, the treeline shifted upward by approximately 50 meters. At medium to high resolution, Rösch et al. (2022) used PlanetScope (3 m) and Sentinel-2 (10 m) imagery from 2020, incorporating texture features from the gray level co-occurrence matrix (GLCM), topographic features, and the canopy height model (CHM) to map the distribution of  
50 mountain pine (*Pinus mugo* ssp. *Mugo Turra*) in the Sarntal Alps. Their study achieved classification accuracies of 90.9% (PlanetScope) and 90.6% (Sentinel-2), demonstrating the value of multi-source data fusion. At very high resolution, Terskaia et al. (2020) combined orthophoto aerial images (1–2 m) from 1952 and 1979 with WorldView-2 imagery (0.5 m resolution) from 2015 to assess shrub and tree encroachment in the western Brooks Range, Alaska. They reported significant changes in vegetation over 63 years, including the loss of tundra and an increase in forest and shrub coverage. While the study reported  
55 percentage changes in land cover types (e.g., an 84% increase in forest), it is essential to note that the reference areas for these changes were derived from historical photo interpretation and may not be directly comparable to current conditions. Collectively, these studies illustrate the potential and versatility of remote sensing at various resolutions and through diverse methods in detecting changes in alpine treeline ecotones. In recent years, with the advancement of remote sensing technology,

many scholars have employed remote sensing imagery to study alpine treelines. Xu et al. (2020) utilized Landsat satellite imagery from 1987 to 2018 for Wuyishan National Park, China. They examined the relationship between treeline position and climate based on the local indicator of spatial autocorrelation (LISA). Their study found that from 1987 to 2018, for every 1°C increase in temperature, the treeline shifted upward by 50 m. Rösch et al. (2022) used 2020 PlanetScope and Sentinel-2 satellite imagery, incorporating texture features from the gray level co occurrence matrix (GLCM), topographic features, and the canopy height model (CHM) to map the distribution of mountain pine (*Pinus mugo* ssp. *Mugo Turra*) in the Sarntal Alps. Their results indicated that combining satellite images with all features could accurately map the distribution of mountain pine forests, with an accuracy of 90.96% for PlanetScope imagery and 90.65% for Sentinel-2 imagery. Terskaia et al. (2020) analyzed the invasion of trees and tall shrubs into the tundra in the western Brooks Range, Alaska, using orthophoto aerial images from 1952 and 1979, along with WorldView 2 satellite imagery from 2015. Their study found that between 1952 and 2015, arctic and alpine tundra areas decreased by 31% and 15%, respectively, while tall shrubs, mixed tree-shrub areas, and forests increased by 86%, 385%, and 84%, respectively. The average treeline was located at an elevation of 202 meters. These studies collectively confirm the reliability of remote sensing technology in researching alpine treeline changes.

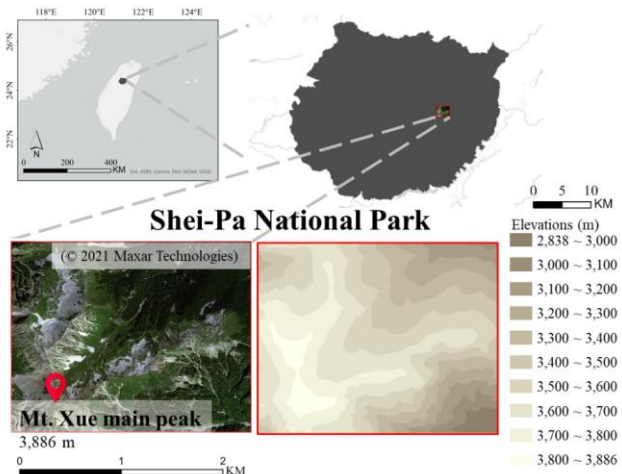
The integration of machine learning with remote sensing has also been successfully applied to forest studies, with many scholars reporting [promising classification results](#) using the Random Forest (RF) and U-Net models. Jombo et al. (2020) used WorldView-2 imagery with RF and Support Vector Machines (SVM) models to classify five types of street trees in the complex urban environment of Randburg [municipality](#), achieving overall accuracies of 84.2% and 81.2%, respectively. Similarly, Jackson and Adam (2021) employed WorldView-2 imagery with RF and SVM to classify endangered tree species in the Mount Kenya Forest Reserve (MKFR), finding that RF outperformed SVM. [Wagner et al. \(2019\) applied a U-Net convolutional network to identify forests in the Atlantic rainforest region of Brazil using ultra-high-resolution WorldView-3 satellite imagery.](#) [Tobias et al. \(2019\) used WorldView-3 imagery to detect oil palm and coconut palm tree distribution in Indonesia.](#) [Freudenberg et al. \(2019\) used WorldView-2 and WorldView-3 imagery in Indonesia to detect Oil and coconut palm tree distribution.](#) In addition to evaluating U-Net's detection accuracy, they assessed its processing speed, finding that the U-Net-based model achieved a maximum throughput of 235 hectares per second at a 40 cm resolution. The model demonstrated high generalizability, with detection accuracies ranging from 89% to 92% across different regions. Their study suggested that this method could be used for rapid nationwide detection of oil palm distribution. [Based on these studies, we conclude that applying high-resolution WorldView satellite imagery combined with RF and U-Net machine learning models offers accuracy, cost efficiency, and generalizability advantages for ecological remote sensing classification.](#) Therefore, this study will integrate WorldView-2 satellite imagery with RF and U-Net models to classify alpine treelines, find important features, and understand the change and spatial patterns in the Xue Mountain glacial cirques region in Taiwan.

## 2 Materials and methods

### 95 2.1 Study site

The Xue Mountain glacial cirques are located in Shei-Pa National Park in north-central Taiwan, covering an area of approximately 4 km<sup>2</sup>. The central peak of Xueshan has an elevation of 3,886 m. The cirque serves as a crucial habitat for Taiwan's endemic species, the Yushan Juniper (*Juniperus morrisonicola*), Yushan rhododendron (*Rhododendron pseudochrysum*), and the Taiwan fir (*Abies kawakamii*), which is primarily distributed at elevations between 3,000 and 3,600 m. [Most ecological studies conducted in this research area have focused on Taiwan fir forests, with several researchers estimating wood volumes, competitive pressure, forest structure, and spatial distribution of the species primarily through field surveys conducted below the alpine treeline ecotone \(Li et al., 2021; Wang et al., 2021; Chiu et al., 2022; Liao et al., 2023a; Liao et al., 2023b\)](#). In contrast, relatively little attention has been given to the dynamics of treeline ecotone shifts.

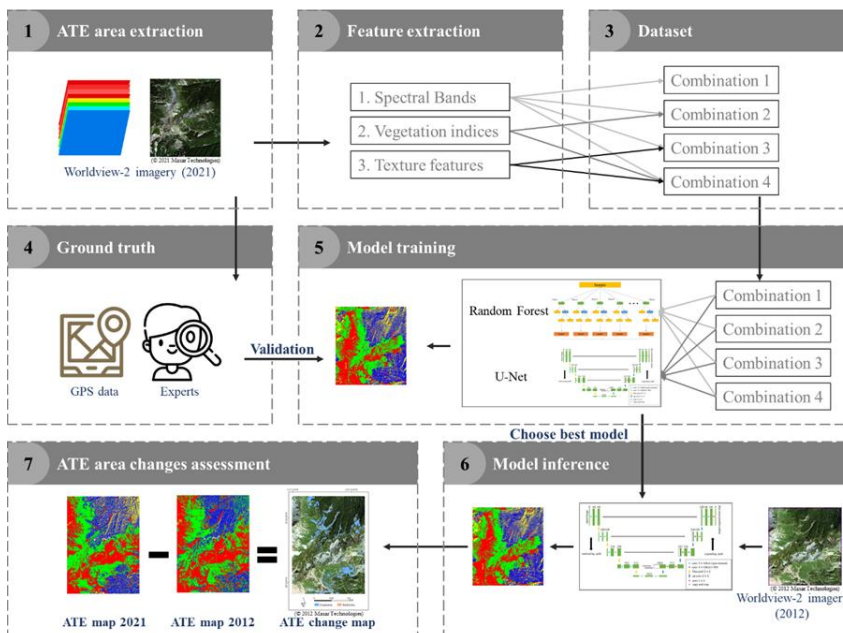
In this study, we define the treeline ecotone not as a fixed linear boundary but as a transitional zone where krummholz, such as Yushan Juniper and Yushan rhododendron, begin to appear within the alpine talus slope (Liao, 2016; Liao et al., 2023a). This ecotone represents an area of ecological transition from subalpine forest to alpine vegetation. Several researchers have been conducting studies on the volume estimation, competitive pressure, forest structure, and spatial distribution of the Taiwan fir, primarily through field surveys (Li et al., 2021; Wang et al., 2021; Chiu et al., 2022; Liao et al., 2023a; Liao et al., 2023b). The study area is shown in Fig. 1.



110 [Figure 1. Geographic location of the treeline ecotone study area in the Xue Mountain glacial cirques in Shei-Pa National Park \(top-right map\) in north-central Taiwan \(top-left map\). The red marker in the Worldview-2 image \(bottom-left map\) indicates the research area. The digital elevation model shown in the bottom-right image shows the same area as the Worldview-2 image and covers the entire study area](#) [Figure 1: study site](#)

## 2.2 Research flow

115 This study utilized WorldView-2 satellite imagery from 2021 to extract raw spectral bands, vegetation indices, and texture features. Starting with the eight spectral bands, vegetation indices, and texture features were sequentially added to form four different feature combinations. Classification models were developed using the RF and U-Net models, and the optimal model is selected. This model is then applied to 2012 imagery to map the distribution of the alpine treeline and analyzed changes over the decade. The research workflow was illustrated in Fig. 2.



120 **Figure 2. Research flow for classifying WorldView-2 images of a treeline ecotone on Mt. Xue in Taiwan to detect treeline changes.** The process begins with WorldView-2 satellite image acquisition, followed by feature extraction (spectral bands, vegetation indices, and texture features), model training using Random Forest (RF) and U-Net, accuracy evaluation, feature selection, and temporal analysis of alpine treeline changes between 2012 and 2021.

## 125 Figure 2: Research flow

The research data sources were categorized into satellite imagery and field surveys, with satellite imagery as the primary source and field surveys used as supplementary validation to ensure the accuracy of the treeline boundary. WorldView-2 was an environmental monitoring satellite operated by Maxar Technologies Inc. (Colorado, USA). It was launched on October 8,

2009, and its geolocation accuracy, even without any ground control points, ~~is reported to be within 3 meters~~<sup>is within 3 meters</sup>. Depending on the  
130 spatial resolution, the revisit time ranges from 1.1 to 3.7 days.

-The satellite ~~provided~~<sup>provides</sup> two imaging modes: panchromatic and multispectral. The spatial resolution ~~was~~<sup>is</sup> 0.41 m in the panchromatic mode, and the spectral range spans 450–800 nm. This mode ~~offered~~<sup>offers</sup> high spatial resolution, allowing for detailed image representation. In the multispectral mode, the spatial resolution ~~was~~<sup>is</sup> 1.64 m, and the spectral range ~~extended~~<sup>extends</sup> from 400 to 1040 nm, covering eight spectral bands, as shown in Table 1. ~~To enhance spatial detail, all multispectral bands were~~  
135 ~~pansharpening using the corresponding high-resolution panchromatic band, yielding a uniform spatial resolution of 0.4 meters across all datasets used for feature extraction. The pansharpened multispectral imagery was the basis for deriving vegetation indices and texture features.~~

~~Two orthorectified, cloud-free WorldView-2 images acquired on November 3, 2012, and September 26, 2021, were obtained from RiChi Technology Co., Ltd. (New Taipei City, Taiwan). Both images were captured in the autumn season when vegetation had entered dormancy, minimizing the influence of phenological variability such as flowering. Histogram matching was applied to ensure radiometric consistency across the two images. In addition, GPS devices were used to record field survey points, which were subsequently used to verify ATE positions and assist in manual ground truth labeling. For this study, two cloud free WorldView-2 orthorectified images with a spatial resolution of 0.4 meters, acquired on November 3, 2012, and September 26, 2021, were obtained through RiChi Technology Co., Ltd. (New Taipei City, Taiwan), and GPS was used to record survey points.~~

Table 1. Spectral characteristics of WorldView-2 satellite bands: Worldview-2 Satellite image band introduction

Band	Spectral range (nm)	Data quantization (Bits)
Costal Blue (CB)	400-450	
Blue (B)	450-510	
Green (G)	510-580	
Yellow (Y)	585-625	
Red (R)	630-690	11
Red Edge (RE)	703-745	
Near Infrared 1 (NIR1)	770-895	
Near Infrared 2 (NIR2)	860-1040	

## 2.4 Vegetation indices Index

格式化: 字型色彩: 自動

The reflectance spectrum of plant leaves can reflect their internal physiological status, such as chlorophyll content, water  
150 content, intercellular spaces, and cell walls. The frequently discussed spectral bands include red (R), the red edge (RE), and the near-infrared (NIR) bands. Derived vegetation indices, such as the Normalized Difference Vegetation Index (NDVI) and

the Enhanced Vegetation Index (EVI), have been widely used (Rouse et al., 1974; Huete et al., 2002). Additionally, some studies have suggested that the blue (B) and green (G) bands can be used to monitor vegetation phenology and forests. For example, indices such as the Green Chromatic Coordinate (GCC) and the Excess Green Index (ExG) have been developed for this purpose (Sonnenstag et al., 2012; Larrinaga and Brotons, 2019). Since image acquisition ~~was is~~ affected by terrain, leading to shadow occurrences that influence classification accuracy, this study also ~~planned plans~~ to adopt the Shadow-Eliminated Vegetation Index (SEVI) (Jiang et al., 2019). This study will utilize 11 vegetation indices, as summarized in Table 2.

**Table 2: Vegetation indices and their formulas. List of vegetation indices and their formulas derived from spectral bands.**

Vegetation Index	Formula	Reference
Difference Vegetation Index (DVI)	$NIR - R$	Richardson and Wiegand, 1977
Enhanced vegetation index (EVI)	$2.5 \times \frac{(NIR - R)}{(NIR + 6 \times R - 7.5 \times B + 1)}$	Huete et al., 2002
Excess Blue Vegetation Index (ExB)	$\frac{1.4 \times B - G}{G + R + B}$	Mao et al., 2003
Excess Green Index (ExG)	$\frac{2 \times G - R - B}{G + R + B}$	Woebbecke et al., 1995
Excess Green minus Excess Red (ExGR)	$ExG - ExR$	Meyer and Neto, 2008
Excess Red Vegetation Index (ExR)	$\frac{1.4 \times R - G}{G + R + B}$	Meyer et al., 1999
The Green Chromatic Coordinate (GCC)	$G/(R + G + B)$	Gillespie et al., 1987
Normalized difference index (NDI)	$\frac{G - R}{G + R}$	Gitelson and Merzlyak, 1994
Normalized difference vegetation index (NDVI)	$\frac{NIR - R}{NIR + R}$	Rouse et al., 1974
Ratio Vegetation Index (RVI)	$\frac{NIR}{R}$	Jordan, 1969
Shadow- Eliminated Vegetation Index (SEVI)	$RVI + f(\Delta) \times \frac{1}{R}$	Jiang et al., 2019

160

## 2.5 Texture Feature

With the improvement in the spatial resolution of satellite imagery, most ground objects are composed of multiple pixels, making the spatial attributes of images increasingly important (Wang et al., 2015). Texture features extract the structural and arrangement properties of ground objects, which describe the spatial attributes of objects in an image. As one of the key features for image interpretation, texture helps distinguish land cover types with similar spectral characteristics. Texture analysis methods can be categorized into spectral, statistical, and structural approaches, with the Gray Level Co-occurrence

Matrix (GLCM) in statistical approaches being the most commonly used (Hsu, 1978). Guo et al. (2020) applied texture features to map the forest-tundra ecotone in central Eurasia. They found that texture-based classification maps performed better than previous methods, achieving an average classification accuracy of 0.826. Similarly, Sibya et al. (2021) used WorldView-2 170 satellite imagery to classify forest species in South Africa. They found that texture features improved overall classification accuracy by approximately 8% compared to vegetation indices and 13% compared to original spectral bands. Their study also observed that a moving window size of  $7 \times 7$  produced the best results. Therefore, this study adopted a  $7 \times 7$  moving window to compute the GLCM matrix for each of the eight bands, analysing seven statistical metrics, resulting in 56 texture features. The seven statistical metrics used in this study are listed in Table 3.

175

**Table 3: Texture Feature and their formulas. Description of texture features calculated using the gray-level co-occurrence matrix (GLCM).**

Texture Feature	Formula	Reference
Contrast (Con)	$\sum_{i,j=0}^{N-1} P_{i,j}(i - j)^2$	Yuan et al., 1991
Dissimilarity (Dis)	$\sum_{i,j=0}^{N-1} P_{i,j} i - j $	Rubner et al., 2002
Energy (Ene)	$\sum_{i,j=0}^{N-1} P_{i,j}^2$	Hall-Beyer, 2017
Entropy (Ent)	$\sum_{i,j=0}^{N-1} P_{i,j}(-\ln P_{i,j})$	Yuan et al., 1991
Homogeneity (Hom)	$\sum_{i,j=0}^{N-1} \frac{P_{i,j}}{1 + (i - j)^2}$	Hall-Beyer, 2017
Mean (M)	$\sum_{i,j=0}^{N-1} iP_{i,j}$	Materka and Strzelecki, 1998
Variance (Var)	$\sum_{i,j=0}^{N-1} P_{i,j}(i - \text{Mean})^2$	Materka and Strzelecki, 1998

$P_{i,j}$  is the gray-level co-occurrence matrix after normalization.

## 2.6 Methods

### 2.6.1 Random Forest (RF)

180 Random Forests (RF) ~~were is~~—an ensemble classifier widely used in remote sensing due to its ability to handle high-dimensional data. It generates multiple decision trees (DTs), where each tree ~~made makes~~—predictions based on observed features through a series of decision-making steps, ultimately concluding the target variable. Decision trees, also known as classification trees, ~~were are~~—a type of predictive model. Random forests ~~used use~~—the Bagging algorithm (Bootstrap Aggregating) as their core classification mechanism. The process ~~began begins~~—by randomly sampling the data to create 185 training datasets. After each sampling, the selected data points ~~were are~~—returned to the dataset for the next round of sampling (bootstrap sampling). This process ~~was is~~—repeated multiple times, resulting in several training datasets, which ~~were are~~—then used to train multiple decision trees. This approach ~~allowed allows~~—for scenarios where specific data points ~~were are~~—sampled multiple times while others may not. Each decision tree ~~selected selects~~—a random subset of features at each node to determine the best split, ultimately generating predictions from each tree. ~~The final classification result is determined by aggregating all~~ 190 ~~decision tree predictions using a majority voting approach. To evaluate the importance of each feature, the Random Forest model uses the Gini Index, which measures the impurity of a node. A lower Gini value indicates better class separation. The Gini Index for a node  $m$  is calculated as follows:~~

$$Gini_m = \sum_{k=1}^K \hat{p}_{mk} (1 - \hat{p}_{mk}) \quad (1)$$

195 Where  $\hat{p}_{mk}$  was the probability of a sample at node  $m$  belonging to class  $k$ , and  $K$  was the total number of classes. The Gini Index also supported the out-of-bag (OOB) error estimation and was commonly used to determine feature importance in classification tasks (Belgiu and Drăguț, 2016; Breiman, 2001; Chen et al., 2023). ~~The final classification result is determined by aggregating all decision tree predictions using a majority voting approach. The model also utilizes the Gini Index, calculated using the following formula: the Gini Index represents the out-of-bag (OOB) error rate. This metric is used to assess the contribution of each feature to the model, serving as an indicator of feature importance (Belgiu and Drăguț, 2016; Breiman, 2001; Chen et al., 2023).~~

### 2.6.2 U-Net

200 Ronneberger et al. (2015) proposed the original U-Net model, which evolved from the fully connected network (FCN) and was initially applied to biomedical image segmentation. The model is named U-Net because its architecture resembles a U-shaped structure. It is also a shallow convolutional neural network (CNN) segmentation model. The U-Net model consists of a contracting path (downsampling) and an expanding path (upsampling). Similar to FCN, U-Net does not have fully connected layers, and its use of convolutional layers significantly reduces the amount of training data required while allowing inputs of different sizes. Before entering the contracting or expanding path, the data undergoes two consecutive convolutional layers, which help the network extract target features more effectively. This process also enhances the integration of fine

details with feature maps, thereby improving segmentation quality. Each convolutional layer is followed by a rectified linear unit (ReLU) activation function, which enhances training efficiency without affecting model accuracy. The pooling layer at the bottom serves as a nonlinear form of downsampling, reducing the spatial size of the data, decreasing the number of parameters and computational costs, and helping to control overfitting. Since U-Net lacks fully connected layers, it effectively minimizes information loss caused by downsampling and preserves finer image details.

### 2.6.3 Data set

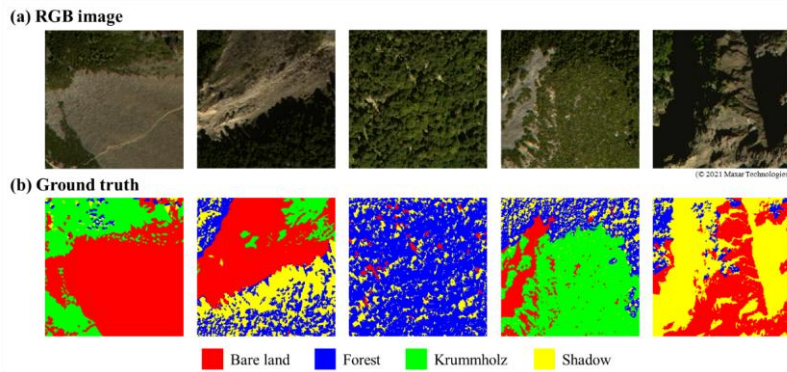
The WorldView-2 satellite imagery consists of eight spectral bands (CB, B, G, Y, R, RE, NIR1, NIR2). Based on these eight bands, this study derived 13 vegetation indices and 56 texture features, resulting in 77 feature variables. The original eight bands were incrementally combined with vegetation indices and texture features, forming four different feature combinations (Table 4), as shown in Table 4.

-Ground truth data in the study area were manually labeled using a pixel-based approach and categorized into four classes: (1) Bare land, referring to areas of exposed soil, rock surfaces, or sparsely vegetated ground; (2) Forest, defined as regions with dense, continuous tree canopy cover; (3) Krummholz, representing stunted, shrub-like trees typically found at high elevations near the treeline and shaped by wind or snow pressure (Liao et al., 2023a); and (4) Shadow, representing regions with low reflectance caused by topographic shading or solar angle effects. The class definitions were established based on visual inspection and field knowledge of the study area (Fig. 3). The labeling process was independent and performed by visually interpreting the pansharpened RGB composite imagery, referencing known terrain characteristics, and assisted by field-collected GPS survey points.

Each image ( $5380 \times 4671$  pixels) was segmented into 110 non-overlapping patches of  $512 \times 512$  pixels. The dataset split was performed at the patch level, not the pixel level, to avoid spatial autocorrelation and data leakage. Specifically, 80% of the patches were randomly selected for training and validation (with a 75/25 split), and the remaining 20% were used as an independent test set. In total, 66 patches were used for training, 22 for validation, and 22 for testing. were labeled using a pixel-based approach and categorized into four classes: bare land, forest, krummholz, and shadow (Fig. 3). Each image ( $5380 \times 4671$  pixels) was segmented into smaller images of  $512 \times 512$  pixels, yielding a total of 110 images. The dataset was randomly split, with 80% used for training and validation and 75% and 25% allocated for training and validation, respectively. The remaining 20% was designated as the test dataset. The number of images used for training, validation, and testing was 66, 22, and 22, respectively.

Table 4. Definitions of the four feature combinations used in model training. The table shows the input feature types and their corresponding dimensionality. Combination of features designed in this study

Feature combinations	Input feature	Feature Dimension
1	spectral band	8
2	spectral band, vegetation indices	21
3	spectral band, texture features	64



240 **Figure 3. Ground truth label generation for land cover classification. (a) WorldView-2 RGB composite image from 2021; (b) manually annotated labels showing four classes: forest, krummholz, bare land, and shadow.** Schematic diagram of ground truth label categories. (a) Original data (RGB image), (b) Ground truth labels.

格式化: 字型色彩: 自動

## 2.6.43 Evaluation Index

245 This study uses overall accuracy (OA), F1-score, and the Kappa coefficient as assessment metrics to evaluate classification accuracy. The formulas for each metric are explained below.

$$OA = \frac{TP+TN}{TP+FP+TN+FN}, \quad (2)$$

$$F1 - score = \frac{2 \times TP}{2 \times TP + FP + FN}, \quad (3)$$

$$Kappa = \frac{P_o - P_e}{1 - P_e}, \text{ with} \quad (4)$$

$$P_o = \frac{TP+TN}{TP+FP+TN+FN}, \text{ and} \quad (5)$$

$$250 P_e = \frac{(TP+FN) \times (TP+FP) + (FP+TN) \times (FN+TN)}{(TP+FP+TN+FN)^2}, \quad (6)$$

Among them,  $TP$  (true positive),  $TN$  (true negative),  $FP$  (false positive), and  $FN$  (false negative).

格式化: 字型色彩: 自動

### 3. Results

#### 3.1 Feature Combination Comparison

255 This study explored four feature combinations, including spectral bands (8 features), vegetation indices (13 features), and texture features (56 features), for classifying bare land, forest, krummholz, and shadow using both RF and U-Net models. The F1-scores, representing the harmonic mean of precision and recall, provided a balanced assessment of classification performance. All classes achieved F1-scores above 0.6 (Fig. 4). Forest and krummholz were more frequently misclassified with one another due to their similar vegetation structures, while bare land and shadow were more easily distinguished, achieving F1-scores above 0.8.

260 Overall, the different feature combinations produced similar classification performance, with only minor differences observed across classes and models. In the RF model, bare land and shadow achieved the highest F1-scores (0.905 and 0.866, respectively) when using Combination 1 (spectral bands only). Forest and krummholz performed slightly better with Combination 4 (spectral bands, vegetation indices, and texture features), achieving F1-scores of 0.827 and 0.776, respectively. In the U-Net model, Combination 1 yielded the best result for bare land ( $F1 = 0.889$ ), while Combination 4 slightly improved 265 the classification of forest (0.828), krummholz (0.886), and shadow (0.869). These findings suggested that incorporating vegetation indices and texture features improved model performance for specific vegetation classes, particularly in the U-Net model, although overall improvements remained relatively modest.

270 The overall accuracy (OA) and Kappa coefficient for each feature combination were summarized in Table 5. Similar to the accuracy patterns for the individual classes, in the U-Net models, the OA improved as the number of features increased, whereas for the RF models this was not the case (Table 5). A consistent increase in OA was observed as more features were incorporated. For both models, Combination 4 yielded the highest OA values: 0.830 for RF and 0.838 for U-Net, representing improvements of 0.011 and 0.085, respectively, over Combination 1. The Kappa coefficients exhibited similar trends, increasing from 0.753 to 0.768 in RF and from 0.666 to 0.778 in U-Net. These results confirmed that both OA and Kappa supported the observed pattern of slightly enhanced classification performance with expanded feature sets. This study explores 275 four feature combinations using spectral bands, vegetation indices, and texture features for classifying bare land, forest, krummholz, and shadow with the RF and U-Net models. The F1-score results are shown in Fig. 4. Overall, the F1-score exceeds 0.6 for all classes. Since forest and krummholz are both vegetation types, they tend to influence each other more, whereas the classification accuracy for bare land and shadow is higher, reaching over 0.8. Comparing the RF and U-Net models, the RF model exhibits more stable F1-score differences across the four feature combinations. In contrast, the U-Net model 280 shows more significant variability in F1-scores.

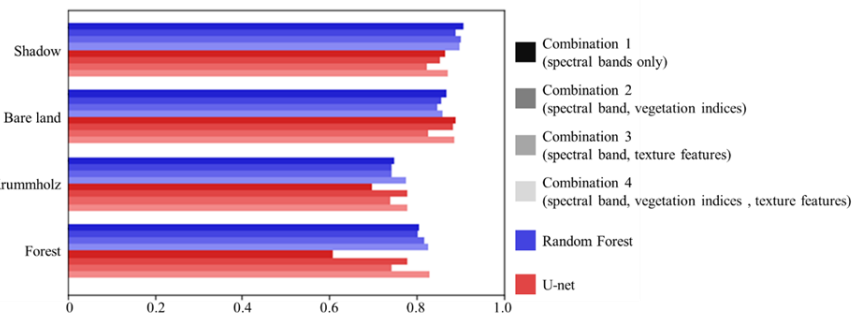


Figure 4. F1-scores for four land cover classes (forest, krummholz, bare land, shadow) using RF and U-Net models with different feature combinations.

Table 5. Evaluation of classification accuracy using different feature combinations and models. Overall accuracy (OA) and Kappa coefficient are shown for Random Forest (RF) and U-Net models. Numbers in parentheses indicate the number of input features. Bold values indicate the best results for each metric.

Feature (DIMs)	Combinations 1(8)		Combinations 2(21)		Combinations 3(64)		Combinations 4(77)	
Method	RF	U-Net	RF	U-Net	RF	U-Net	RF	U-Net
OA	0.819	0.753	0.817	0.780	0.812	0.819	0.830	<b>0.838</b>
Kappa	0.753	0.666	0.751	0.703	0.743	0.755	0.768	<b>0.778</b>

### 3.2 Feature Importance Selection Based on Random Forest Model

The upper limit of the ATE was determined based on the spatial distribution boundary where patches of forest transitioned into krummholz and bare land. This boundary reflected a gradual to abrupt ecological shift in vegetation types and was identified using classification results derived from satellite imagery. To ensure accuracy, these results were cross-validated with GPS-based field survey points. Since forest classification accuracy played a key role in delineating this boundary, particular emphasis was placed on improving forest classification performance. Therefore, after integrating the results from Section 3.1, further analysis was conducted using Feature Combination 4 and the U-Net model. As the number of features increased, model training times also lengthened, making it necessary to evaluate both classification accuracy and computational cost. To address this, the study employed the feature importance ranking function of the RF model to the 77 features (Fig. 5). Based on the cumulative model interpretability results, 95% cumulative interpretability was achieved using 61 features. Further analysis revealed that the most important features, according to the ranking, were SEVI, Y, B, G, and NDVI2. In contrast, texture features were relatively less important, as also suggested by the low F1 scores for combination 3 (spectral, texture; Fig. 4). However, for the forest class in particular, texture features significantly improved classification

格式化: 字型色彩: 自動

格式化: 字型色彩: 自動

accuracy compared to using only spectral bands, and the inclusion of vegetation indices contributed even more to the performance.

Using the top 61 selected features based on feature importance, a retraining process was carried out. The classification results remained similar before and after feature selection (Fig. 6), while training time was reduced by 14.3%. Although improving computational efficiency was not the primary objective, feature selection helps achieve model parsimony, balancing model complexity with performance, which in turn enhances interpretability and generalization. Notably, the overall accuracy and Kappa coefficient increased slightly by 0.4% (Table 6). While the numerical gain may appear small, such improvement is relevant in ecological applications where even minor increases in accuracy can enhance the detection of subtle land cover changes, such as shifts in forest boundaries over time. The treeline is determined based on the boundary between bare land, forests, and krummholz. Therefore, after integrating the results from Section 3.1, further analysis was conducted using Feature Combinations 4 and the U-Net model. Since an increase in the number of features leads to longer model training times, it is necessary to evaluate both classification accuracy and computational time costs. To address this, this study utilized the feature importance ranking function of the RF model to rank the importance of the 77 features. The feature ranking results are shown in Fig. 5. Based on cumulative model interpretability, 95% cumulative interpretability can be obtained by 61 features. Further analysis revealed that according to the ranking, the most important features were SEVI, Y, B, G, and NDVI2.

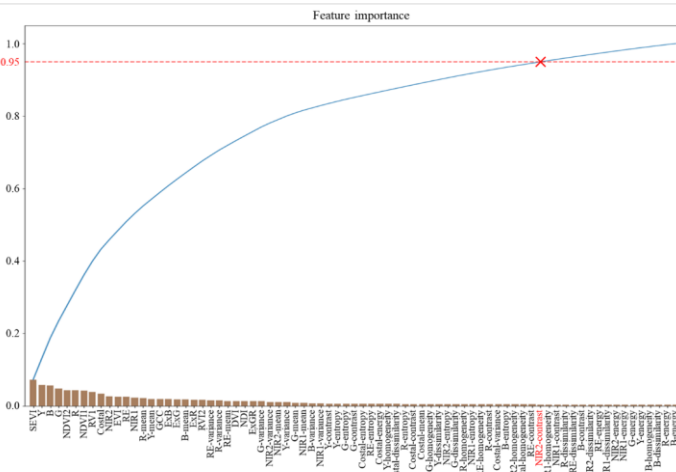


**Figure 5. Feature importance ranking derived from the Random Forest model.** Features are ranked based on their contribution to classification accuracy, with the top-ranked features including SEVI, Y (yellow), B (blue), G (green), and NDVI2. Most of the top features are spectral bands and vegetation indices, while texture features rank lower.

**Table 6. Comparison of model performance before and after feature selection.** Training time is presented in hours. The results show reduced training time and slightly improved classification accuracy after feature selection.

	Without feature selection	With feature selection	Difference (%)
Training time(hr)	7.70827750	6.60823789	-14.3
time(s)			
OA	0.838	0.842	+0.4
Kappa	0.778	0.784	+0.4

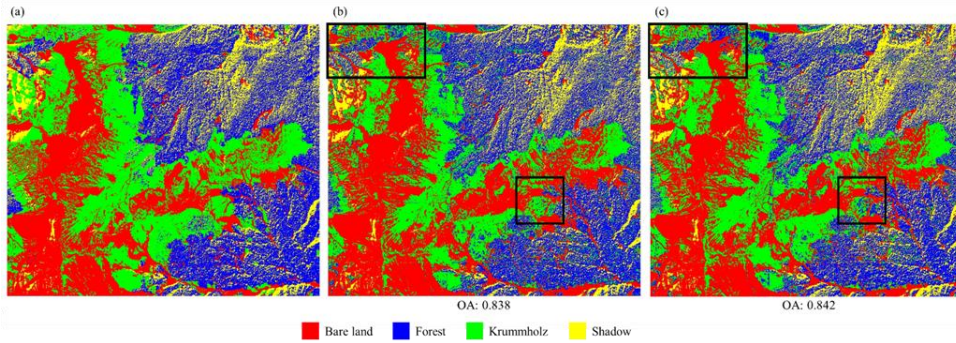


Figure 6: Comparison of 2021 image classification results before and after feature selection. (a) Ground truth; (b) model result using 77 features; (c) model result using 61 features.

Figure 6: Model classification results with/without feature selection (a) Ground truth (b) Without feature selection (c) With feature selection

### 3.3 Decade changes of in the treeline ecotone

A U-Net model was trained using 61 selected features derived based on feature importance. The trained model was applied

330 to classify satellite images from 2012 and 2021. The classification results were validated against field survey data collected in 2021, which recorded vegetation types and the position of the tree line along an elevational gradient. As shown in Fig. 7, the tree line derived from the classification closely aligns well with the tree line identified through GPS-based field survey points.

Over the decade, the proportion of forest area increased by 3.4%, indicating a trend of forest expansion. Meanwhile, the proportion of shadow area also increased by 8.5%; however, this is likely due to differences in lighting conditions and satellite

335 viewing angles between the 2012 and 2021 image acquisitions rather than an actual ecological change. Additionally, krummholz and bare land areas decreased by 3.2% and 8.7%, respectively (Table 7). For the forest category, the forest area expanded by 0.105 km<sup>2</sup> and was reduced by 0.004 km<sup>2</sup> between 2012 and 2021 (Fig. 8). Based on the 95th percentile of DEM elevation values of all pixels classified as forest (Fig. 9), the treeline showed an upward shift of 32.00 meters between 2012 and 2021. The 95% confidence interval ( $\pm 4.00$  meters) was estimated using a bootstrap resampling method (5,000 iterations).

340 Differences in area changes across various elevation ranges are detailed in Table 8, with the most significant changes occurring

格式化: 字型色彩: 自動

格式化: 字型色彩: 自動

格式化: 字型色彩: 自動

in the 3,600- to 3,700-m range, which corresponds to the primary treeline ecotone change zone in the Xue Mountain region. In comparison, the most stable area was observed in the 3,700 to 3,800 m range, where minimal forest presence was detected in both 2012 and 2021, reflecting physiological limits of trees. A U-Net model was trained using 61 selected features based on feature importance, and the trained model was then used to classify the images from 2012 and 2021. The classification results from 2012 and 2021 were compared with field survey data, as shown in Fig. 7. The results indicate that the tree line derived from the classification aligns with the tree line edge identified in the field survey. Over a decade, the proportion of forest and shadow areas increased by 3.4% and 8.5%, respectively, while krummholz decreased by 3.2% and bare land decreased by 8.7% (Table 7). For the forest category, changes in forest area showed an expansion of 0.105 km<sup>2</sup> and a reduction of 0.004 km<sup>2</sup> between 2012 and 2021 (Fig. 8). The elevation distribution of the forest area shifted from 3,699 m to 3,713 m, reflecting a 14 m rise, as shown in Table 8. The differences in area changes across different elevation ranges are detailed in Table 9, with the most significant changes occurring in the 3,500 to 3,600 m range. In comparison, the most stable area was observed in the 3,700 to 3,800 m range.

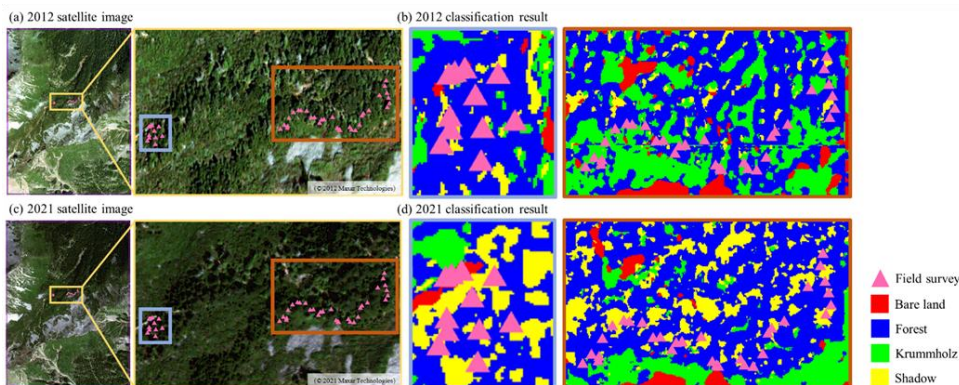


Figure 7 Comparison of satellite imagery and classification results from 2012 and 2021. Panels (a) and (c) show high-resolution satellite images for 2012 and 2021, respectively. Colored boxes in these images indicate the enlarged areas shown in (b) and (d). Panels (b) and (d) present the classification results of the corresponding enlarged regions using a U-Net model trained with 61 selected features. Triangles mark field survey locations.

Table 7. Percentage of each land cover class in 2012 and 2021 classification results. Forest and shadow areas increased over time, while krummholz and bare land decreased.

Classification percentage (%)	Year		Increment / Decrement
	2012	2021	
Forest	22.5	25.9	+3.4
Krummholz	36.4	33.2	-3.2

Bare land	38.1	29.4	-8.7
Shadow	3.0	11.5	+8.5
Total	100	100	

360

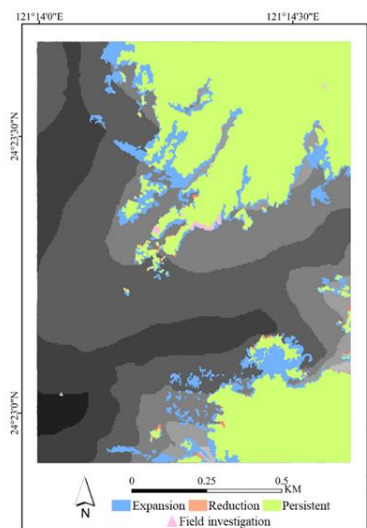
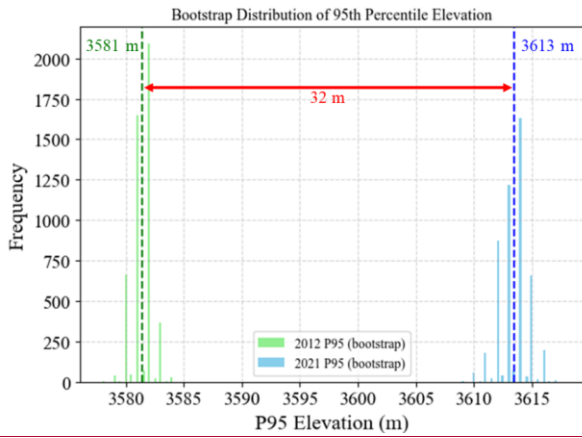


Figure 8. The spatial distribution of forest area changes from 2012 to 2021. Forest expansion is marked in blue, reduction is marked in orange, and persistent is marked in green.

格式化: 字型色彩: 自動



365 **Figure 9. Bootstrap distribution of the 95th percentile elevation of forest cover for 2012 and 2021. The histogram shows the frequency of estimated 95th percentile elevations (P95) based on resampling. Green bars represent 2012 estimates, while blue bars represent 2021. The dashed vertical lines indicate the mean P95 value for each year.**

**Figure 8: Forest area changes in 2021 and 2012**

Elevations (m)	Forest Area in 2012 (ha)	Expansion area (ha)	Reduction area (ha)	Net Change (ha)	Change (%)
3300~3400	6.99	0.28	0.03	0.25	3.6
3400~3500	12.43	2.21	0.08	2.13	17.1
3500~3600	8.40	5.10	0.23	4.87	58.0
3600~3700	3.26	2.88	0.06	2.82	86.4
3700~3800	0.78	0.02	0.00	0.02	2.5

Elevations (m)	Expansion area (km <sup>2</sup> )	Reduction area (km <sup>2</sup> )
3300~3400	0.0028	0.0003
3400~3500	0.0221	0.0008
3500~3600	0.0510	0.0023
3600~3700	0.0288	0.0006
3700~3800	0.0002	0.0000

格式化: 字型色彩: 自動  
 格式化: 字型色彩: 自動

## 4. Discussion

### 4.1 Treeline change and spatial pattern

Our findings reveal that, from 2012 to 2021, the alpine treeline ecotone (ATE) in the Xue Mountain glacial cirque experienced an upward shift of  $32.00 \pm 4.00$  meters, along with a pronounced densification of forest cover. This finding aligns with patterns observed in other mountainous regions worldwide. For example, in Taiwan's Hehuan Mountain and Yushan, similar upward shifts in treeline position and increases in forest density have been reported (Greenwood et al., 2014; Chung et al., 2021). Likewise, Davis et al. (2020) observed an upslope advance of  $0.83 \pm 0.67$  m/year for several tree species in the Rocky Mountains of Canada. In contrast, studies in the European Alps have noted significant reductions in snow cover and increased alpine vegetation productivity, potentially enhancing local carbon sequestration, although with a limited global impact (Rumpf et al., 2022). Additionally, in the eastern Himalayas, over 80% of trees have already reached the thermal treeline, with projected upslope migration of 140 meters by the end of the 21st century due to warming (Wang et al., 2022). These comparisons support the robustness of our observed treeline dynamics and highlight both global consistency and regional variation in alpine ecosystems response to climate change.

Observing the ecological processes and changes of the alpine treeline (ATE) can help assess the impacts of climate change in different regions. In the Rocky Mountains of Canada, Davis et al. (2020) investigated the changes in four tree species (*Abies lasiocarpa*, *Larix lyallii*, *Picea engelmannii*, *Pinus albicaulis*). They found that overall forest stand density increased, with tree distribution advancing upslope toward the treeline at an average rate of  $0.83 \pm 0.67$  m/year. In the European Alps, researchers observed a significant reduction in snow cover. At the same time, the productivity of alpine treeline vegetation increased, enhancing the ability to sequester atmospheric CO<sub>2</sub> and mitigating the effects of climate change (Rumpf et al., 2022). In the Himalayas of Asia, climate impacts have led to more than 80% of trees in the eastern region reaching the thermal treeline, the potential upper range limit set by the growing season temperature. It is predicted that by the end of the 21st century, trees in the east region will migrate upslope by 140 meters (Wang et al., 2022). Similarly, in Taiwan's Hehuan Mountain and Yushan, studies have also found that alpine treelines are shifting to higher elevations, accompanied by a significant increase in forest density (Greenwood et al., 2014; Chung et al., 2021). This study also found that the alpine treeline's elevation in the Xue Mountain glacial cirque increased by 14 meters between 2012 and 2021, which aligns with the findings of previous studies.

### 4.2 Feature importance

In this study, we derived 77 features from satellite imagery, including eight spectral bands, 13 vegetation indices, and 56 texture features. To improve model efficiency, we applied feature importance ranking using the Random Forest (RF) model and selected the top 61 features, which accounted for 95% of the cumulative importance. Among them, SEVI, Yellow (Y), Blue (B), Green (G), and NDVI2 were identified as the most important for classifying the treeline ecotone. Notably, most of these were spectral or vegetation index features, while texture features contributed less. This feature selection not only reduced

405 training time by 14.3% but also slightly improved the overall accuracy (+0.4%) and Kappa coefficient. While OA was used as the primary selection criterion, we also confirmed that these top-ranked features maintained or improved F1-scores for the forest class, which is the primary concern in detecting treeline changes. We recognize that the process of optimizing OA values may sometimes overlook minority or ecologically important classes. Therefore, we specifically examined the F1-score for the forest class—our primary concern for treeline detection—and verified that its classification performance was not compromised. This indicates that our feature selection strategy effectively balanced overall model performance with the accuracy of the most ecologically relevant land-cover category.

410 These findings align with previous studies on vegetation classification using multispectral satellite imagery, though the most informative spectral bands may vary depending on the sensor, study region, and forest type. For instance, studies using Sentinel-2 imagery (10–20 m resolution) found the shortwave infrared (SWIR), red, and near-infrared (NIR) bands to be particularly effective in forest classification tasks. Bolyn et al. (2018) identified SWIR, red, and NIR as the most important features for classifying forest types, while Immitzer et al. (2019) emphasized the role of red and NIR in time-series-based tree species mapping. Similarly, Hościlo and Lewandowska (2019) reported improved forest type discrimination when using multi-temporal red, NIR, and red-edge bands. In contrast, studies using WorldView-2 imagery (high-resolution, 0.4–1.6 m) revealed different key spectral bands. Abutaleb et al. (2021) found that the green, yellow, red, and NIR2 bands were most relevant for mapping eucalyptus trees in a subtropical environment. On the other hand, Immitzer et al. (2012) reported that blue, green, red, and NIR1 bands were particularly effective in classifying coniferous forest types in Austria.

420 These variations underscore the contextual nature of feature importance, suggesting that optimal band selection depends on factors such as spatial resolution, vegetation structure, and topographic complexity. Our results—emphasizing SEVI, Y, B, G, and NDVI2—are well-suited to the alpine treeline environment of Taiwan, where coniferous species such as *Abies kawakamii* dominate. A total of 77 features were derived from the satellite images, including eight spectral bands, 13 vegetation indices, and 56 texture features. Different features have varying degrees of importance for image classification; therefore, an analysis of feature importance must be conducted based on the classification target. In the alpine treeline (ATE) of Xue Mountain, the primary tree species is Taiwan fir (*Abies kawakamii*), which belongs to coniferous forests. Numerous studies have explored the contribution of satellite image bands to conifer species classification and forest land cover mapping. Several researchers using Sentinel 2 imagery have found that shortwave infrared, red, and near-infrared bands are particularly suitable for identifying land cover and different tree species, with the red band being the most effective for coniferous tree indices (Bolyn et al., 2018; Immitzer et al., 2019; Hościlo and Lewandowska, 2019). Using WorldView-2 imagery to study Johannesburg, South Africa, other researchers identified the green, yellow, red, and near infrared 2 bands as the most critical features for vegetation classification (Abutaleb et al., 2021). Similarly, a study classifying natural forests based on WorldView-2 images in eastern Austria found that the blue, green, red, and near infrared 1 bands were the most significant (Immitzer et al., 2012). In this study, the most important bands identified were SEVI, Y, B, G, and NDVI2. Most top-ranked features were spectral bands and vegetation indices, while texture features were less important. Based on these findings, this study concludes that the importance of features varies depending on the region characteristics and classification target.

## 5. Conclusions

This study investigates changes in the ATE of the Xue Mountain glacial cirques in Taiwan from 2012 to 2021, utilizing WorldView-2 imagery in conjunction with Random Forest and U-Net models. By incorporating spectral bands, vegetation indices, and texture features, we achieved improved classification accuracy and computational efficiency. Feature selection identified the most important variables as the Shadow-Eliminated Vegetation Index (SEVI), Yellow (Y), Blue (B), Green (G) bands, and Normalized Difference Vegetation Index (NDVI2). The treeline was defined not as a fixed linear boundary but as a transitional ecotone where krummholz species—such as Yushan juniper (*Juniperus morrisonicola*) and Yushan rhododendron (*Rhododendron pseudochrysanthum*)—begin to appear within the alpine talus slope. This delineation was based on both satellite classification results and GPS-referenced field survey data. Over the past decade, forest cover in the study area expanded by approximately 0.101 km<sup>2</sup>, indicating both denser canopy growth and outward expansion. In addition, the upper limit of forest distribution rose by  $32.00 \pm 4.00$  meters, indicating an upslope shift of the treeline at higher elevations. These findings provide new insights into treeline dynamics in Taiwan's alpine environment and demonstrate the potential of high-resolution satellite imagery for long-term ecological monitoring. This study investigates the changes in the ATE of the Xue Mountain glacial cirques in Taiwan between 2012 and 2021. Specifically, the study employs the RF and U-Net models to generate classification maps of the ATE and analyse changes in bare land, forest, krummholz, and shadow areas based on WorldView-2 satellite imagery-derived vegetation indices and texture features. The results show that incorporating vegetation indices and texture features alongside the spectral bands improves classification accuracy. The best result is the U-Net model with OA 0.838, which is 0.085 higher than the model using spectral bands alone, and the Kappa coefficient is 0.112 higher. With the selection of feature importance, training time was reduced by 14.3%, with a slight improvement in accuracy. The most significant features were SEVI, Y, B, G, and NDVI2. Comparing the classification results from 2012 and 2021 with field surveys, the treeline edges in the classification maps aligned well with surveyed locations. Over a decade, the spatial coverage of trees increased by approximately 0.101 km<sup>2</sup>, indicating a denser forest situation. Additionally, the elevation of forest distribution is found in higher elevations (rise by 14 meters), representing a gradual upward treeline shift. The most significant changes occurred between 3,500 m and 3,600 m, while the 3,700 m to 3,800 m range remained relatively stable. These findings provide essential scientific insights for future ecosystem management in Xue Mountain and demonstrate the effectiveness of satellite imagery in monitoring alpine treeline ATE dynamics, highlighting its significance for biodiversity conservation and sustainable environmental development.

## Data availability

Data are available upon request from the corresponding author (Hui Ping Tsai).

#### Author contributions

Conceptualization, GGW, MCL, WW, HPT and HYT; methodology, GGW, MCL, WW, HPT and HYT; software, GGW, and HPT; validation, GGW, MCL, WW, HPT and HYT; formal analysis, GGW, HPT and HYT; investigation, GGW, MCL, WW, HPT and HYT; resources, MCL, HPT and HYT; data curation, GGW, MCL and WW; writing—original draft preparation, 470 GGW and HPT; writing—review and editing, MCL, HPT and HYT; visualization, GGW and HPT; supervision, HPT and HYT; project administration, HPT and HYT; funding acquisition, MCL, HPT and HYT. All authors have read and agreed to the published version of the manuscript.

#### Competing interests

The authors declare that they have no conflict of interest.

475

This work was partially financially supported by the "Innovation and Development Center of Sustainable Agriculture" from The Featured Areas Research Center Program within the framework of the Higher Education Sprout Project by the Ministry of Education (MOE) in Taiwan. Additionally, the support also provided by the National Science and Technology Council under projects 111-2313-B-054-001, 112-2321-B-005-007-, 112-2634-F-005-002-, 112-2119-M-005-001-, 112-480 2121-M-005-003-, 113-2321-B-005-005-, 113-2634-F-005-002-, 113-2119-M-005-001-, 113-2121-M-005-005- and Shei-Pa National Park Headquarters, National Park Service, Ministry of the Interior under project SP113110.

Abutaleb, K., Newete, S. W., Mangwanya, S., Adam, E., and Byrne, M. J.: Mapping eucalypts trees using high resolution multispectral images: A study comparing WorldView 2 vs. SPOT 7. Egypt. J. Remote Sens. Space Sci., 24(3), 333-342, 485 https://doi.org/10.1016/j.ejrs.2020.09.001, 2021.

Bader, M. Y., Llambí, L. D., Case, B. S., Buckley, H. L., Toivonen, J. M., Camarero, J. J., Cairns, D. M., Brown, C. D., Wiegand, T., and Resler, L. M.: A global framework for linking alpine-treeline ecotone patterns to underlying processes. Ecography, 44(2), 265-292, https://doi.org/10.1111/ecog.05285, 2021.

Belgiu, M., and Drăgut, L.: Random forest in remote sensing: A review of applications and future directions. ISPRS J. Photogramm. Remote Sens. 114, 24-31, https://doi.org/10.1016/j.isprsjprs.2016.01.011, 2016.

Bolyn, C., Michez, A., Gaucher, P., Lejeune, P., and Bonnet, S.: Forest mapping and species composition using supervised per pixel classification of Sentinel-2 imagery. Biotechnol. Agron. Soc., 22(3), https://doi.org/10.25518/1780-4507.16524, 2018.

Boutaba, R., Salahuddin, M. A., Limam, N., Ayoubi, S., Shahriar, N., Estrada-Solano, F., and Caicedo, O. M.: A comprehensive survey on machine learning for networking: evolution, applications and research opportunities. J. Internet Serv. Appl., 9(1), 1-99, https://doi.org/10.1186/s13174-018-0087-2, 2018.

Breiman, L.: Random forests. Mach. Learn., 45, 5-32, https://doi.org/10.1023/A:1010933404324, 2001.

Chen, J., Tan, R., and Yang, Y.: Research on an innovative feature importance recognition algorithm based on GINI-OOB index, in 2023 IEEE International Conference on Image Processing and Computer Applications (ICIPCA), Changchun, 500 China, 862-866, <https://doi.org/10.1109/ICIPCA59209.2023.10257830>, 2023.

Chen, W., Ding, H., Li, J., Chen, K., and Wang, H.: Alpine treelines as ecological indicators of global climate change: Who has studied? What has been studied?. *Ecol. Inform.*, 70, 101691, <https://doi.org/10.1016/j.ecoinf.2022.101691>, 2022

Chiu, C. A., Tzeng, H. Y., Lin, C. T., Chang, K. C., and Liao, M. C.: Spatial distribution and climate warming impact on *Abies kawakamii* forest on a subtropical island. *Plants*, 11(10), 1346, <https://doi.org/10.3390/plants11101346>, 2022.

Chung, M. E., Doyog, N. D., and Lin, C.: Monitoring of the trend of timberlines in Taiwan amidst climate change through multi-temporal satellite images, in 2021 IEEE International Geoscience and Remote Sensing Symposium IGARSS, 505 Brussels, Belgium, 6488-6491, <https://doi.org/10.1109/IGARSS47720.2021.9553538>, 2021.

Davis, E. L., Brown, R., Daniels, L., Kavanagh, T., and Gedalof, Z. E.: Regional variability in the response of alpine treelines to climate change. *Clim. Change*, 162(3), 1365-1384, <https://doi.org/10.1007/s10584-020-02743-0>, 2020.

Du, H., Liu, J., Li, M. H., Büntgen, U., Yang, Y., Wang, L., Wu, Z., and He, H. S.: Warming-induced upward migration of the alpine treeline in the Changbai Mountains, northeast China. *Global Change Biol.*, 24(3), 1256-1266, 510 <https://doi.org/10.1111/gcb.13963>, 2018.

Engler, R., Randin, C. F., Thuiller, W., Dullinger, S., Zimmermann, N. E., Araújo, M. B., Pearman, P. B., Lay, G. L., Piedallu, C., Albert, C. H., Choler, P., Coldea, G., Lamo, X. D., Dirnböck, T., Gégout, J. C., Gómez-García, D., Grytnes, J. A., 515 Heegaard, E., Høistad, F., Nogués-Bravo, D., Normand, S., Puçaş, M., Sebastià, M. T., Stanisci, A., Theurillat, J. P., Trivedi, M. R., Vittoz, P., and Guisan, A.: 21st century climate change threatens mountain flora unequally across Europe. *Global Change Biol.*, 17(7), 2330-2341, <https://doi.org/10.1111/j.1365-2486.2010.02393.x>, 2011.

Freudenberg, M., Nölke, N., Agostini, A., Urban, K., Wörgötter, F., and Kleinn, C.: Large scale palm tree detection in high resolution satellite images using U-Net. *Remote Sens.*, 11(3), 312, <https://doi.org/10.3390/rs11030312>, 2019.

Garbarino, M., Morresi, D., Anselmetto, N., and Weisberg, P. J.: Treeline remote sensing: from tracking treeline shifts to multi-dimensional monitoring of ecotonal change. *Remote Sens. Ecol. Conserv.*, 9(6), 729-742, 520 <https://doi.org/10.1002/rse2.351>, 2023.

Gillespie, A. R., Kahle, A. B., and Walker, R. E.: Color enhancement of highly correlated images. II. Channel ratio and “chromaticity” transformation techniques. *Remote Sens. Environ.*, 22(3), 343-365, [https://doi.org/10.1016/0034-4257\(87\)90088-5](https://doi.org/10.1016/0034-4257(87)90088-5), 1987.

Gitelson, A., and Merzlyak, M. N.: Spectral reflectance changes associated with autumn senescence of *Aesculus hippocastanum* L. and *Acer platanoides* L. leaves. Spectral features and relation to chlorophyll estimation. *J. Plant Physiol.*, 143(3), 286-292, [https://doi.org/10.1016/S0176-1617\(11\)81633-0](https://doi.org/10.1016/S0176-1617(11)81633-0), 1994.

Greenwood, S., Chen, J. C., Chen, C. T., and Jump, A. S.: Strong topographic sheltering effects lead to spatially complex 525 treeline advance and increased forest density in a subtropical mountain region. *Glob. Change Biol.*, 20(12), 3756-3766, <https://doi.org/10.1111/gcb.12710>, 2014.

Guo, W., Rees, G., and Hofgaard, A.: Delineation of the forest-tundra ecotone using texture-based classification of satellite imagery. *Int. J. Remote Sens.*, 41(16), 6384-6408, <https://doi.org/10.1080/01431161.2020.1734254>, 2020.

Hall-Beyer, M.: GLCM Texture: A Tutorial v. 3.0 March 2017, 2017.

535 Hościlo, A., and Lewandowska, A.: Mapping forest type and tree species on a regional scale using multi-temporal Sentinel-2 data. *Remote Sens.*, 11(8), 929, <https://doi.org/10.3390/rs11080929>, 2019.

Hsu, S. Y.: Texture-tone analysis for automated land-use mapping. *Photogramm. Eng. Remote Sens.*, 44(11), 1393-1404, 1978.

Huete, A., Didan, K., Miura, T., Rodriguez, E. P., Gao, X., and Ferreira, L. G.: Overview of the radiometric and biophysical performance of the MODIS vegetation indices. *Remote Sens. Environ.*, 83(1-2), 195-213, [https://doi.org/10.1016/S0034-4257\(02\)00096-2](https://doi.org/10.1016/S0034-4257(02)00096-2), 2002

540 Huss, M., Bookhagen, B., Huggel, C., Jacobsen, D., Bradley, R. S., Clague, J. J., Vuille, M., Buytaert, W., Cayan, D. R., Greenwood, G., Mark, B. G., Milner, A. M., Weigertner, R., and Winder, M.: Toward mountains without permanent snow and ice. *Earth's Future*, 5, 418-435, <https://doi.org/10.1002/2016EF000514>, 2017.

Immitzter, M., Atzberger, C., and Koukal, T.: Tree species classification with random forest using very high spatial resolution 8-band WorldView-2 satellite data. *Remote Sens.*, 4(9), 2661-2693, <https://doi.org/10.3390/rs4092661>, 2012.

545 Immitzter, M., Neuwirth, M., Böck, S., Brenner, H., Vuolo, F., and Atzberger, C.: Optimal input features for tree species classification in Central Europe based on multi-temporal Sentinel-2 data. *Remote Sens.*, 11(22), 2599, <https://doi.org/10.3390/rs11222599>, 2019.

Jackson, C. M., and Adam, E.: Machine learning classification of endangered tree species in a tropical submontane forest using worldview-2 multispectral satellite imagery and imbalanced dataset. *Remote Sens.*, 13(24), 4970, <https://doi.org/10.3390/rs13244970>, 2021.

Jiang, H., Wang, S., Cao, X., Yang, C., Zhang, Z., and Wang, X.: A shadow-eliminated vegetation index (SEVI) for removal of self and cast shadow effects on vegetation in rugged terrains. *Int. J. Digit. Earth*, 12(9), 1013-1029, <https://doi.org/10.1080/17538947.2018.1495770>, 2019.

550 Johnson, J. S., Gaddis, K. D., Cairns, D. M., and Krutovsky, K. V.: Seed dispersal at alpine treeline: An assessment of seed movement within the alpine treeline ecotone. *Ecosphere*, 8(1), e01649, <https://doi.org/10.1002/ecs2.1649>, 2017.

Jombo, S., Adam, E., Byrne, M. J., and Newete, S. W.: Evaluating the capability of Worldview-2 imagery for mapping alien tree species in a heterogeneous urban environment. *Cogent Soc. Sci.*, 6(1), 1754146, <https://doi.org/10.1080/23311886.2020.1754146>, 2020.

560 Jordan, C. F.: Derivation of leaf-area index from quality of light on the forest floor. *Ecol.*, 50(4), 663-666, <https://doi.org/10.2307/1936256>, 1969

Körner, C., and Hoch, G.: Not every high-latitude or high-elevation forest edge is a treeline. *J. Biogeogr.*, 50(5), 838-845, <https://doi.org/10.1111/jbi.14593>, 2023.

Körner, C.: Treelines will be understood once the functional difference between a tree and a shrub is. *Ambio*, 41(Suppl 3), 565 197-206, <https://doi.org/10.1007/s13280-012-0313-2>, 2012.

Kuo, C. C., Liu, Y. C., Su, Y., Liu, H. Y., and Lin, C. T.: Responses of alpine summit vegetation under climate change in the transition zone between subtropical and tropical humid environment. *Sci. Rep.*, 12(1), 13352, <https://doi.org/10.1038/s41598-022-17682-2>, 2022.

Larrinaga, A. R., and Brotons, L.: Greenness indices from a low-cost UAV imagery as tools for monitoring post-fire forest recovery. *Drones*, 3(1), 6, <https://doi.org/10.3390/drones3010006>, 2019

570 Li, M. H., Jiang, Y., Wang, A., Li, X., Zhu, W., Yan, C. F., Du, D., Shi, Z., Lei, J., Schönbeck, L., He, P., Yu, F. H., and Wang, X.: Active summer carbon storage for winter persistence in trees at the cold alpine treeline. *Tree Physiolo.*, 38(9), 1345-1355, <https://doi.org/10.1093/treephys/tpy020>, 2018.

575 Li, P. H., Liao, M. C., Tzeng, H. Y., Tseng, Y. H., and Yen, T. M.: Applicability evaluation of tree volume equation for *Abies kawakamii* (Hayata) Ito based on stem analysis data in Taiwan. *J. For. Res.*, 26(5), 336-343, <https://doi.org/10.1080/13416979.2021.1927502>, 2021.

Liao, M. C. Vegetation Structure of Subalpine Ecosystem in Taiwan: A Case Study of Xue Mountain. Unpublished doctoral dissertation. National Chung Hsing University, 2016

580 Liao, M. C., Wang, W., and Tzeng H. Y.: Study of the Structure and Competitive Coexistence of Subalpine Krummholz Species in Taiwan. *Taiwan J. For. Sci.*, 38(3), 203-220, [https://doi.org/10.7075/TJFS.202309\\_38\(3\).0002](https://doi.org/10.7075/TJFS.202309_38(3).0002), 2023a.

Liao, M. C., Li, P. H., Wang, W., Chiu, C. A., and Tzeng, H. Y.: Structure changes of the subalpine Taiwan fir (*Abies kawakamii* (Hay.) Ito) forest from 2008 to 2018. *J. For. Res.*, 28(2), 126-135, <https://doi.org/10.1080/13416979.2022.2135523>, 2023b.

585 Lin, J. C., Chiou, C. R., Chan, W. H., and Wu, M. S.: Valuation of forest ecosystem services in Taiwan. *Forests*, 12(12), 1694, <https://doi.org/10.3390/f12121694>, 2021.

Loranger, H., Zott, G., and Bader, M. Y.: Early establishment of trees at the alpine treeline: Idiosyncratic species responses to temperature-moisture interactions. *AoB Plants*, 8, plw053, <https://doi.org/10.1093/aobpla/plw053>, 2016.

Mao, W., Wang, Y., and Wang, Y.: Real-time detection of between-row weeds using machine vision. In: 2003 ASAE Annual Meeting (p. 1). American Society of Agricultural and Biological Engineers, <https://doi.org/10.13031/2013.15381>, 2003

590 Materka, A., and Strzelecki, M.: Texture analysis methods—a review. Technical University of Lodz, Institute of Electronics, COST B11 Report, Brussels, 9–11, 1998

Meyer, G. E., and Neto, J. C.: Verification of color vegetation indices for automated crop imaging applications. *Comput. Electron. Agric.*, 63(2), 282-293, <https://doi.org/10.1016/j.compag.2008.03.009>, 2008.

Meyer, G. E., Hindman, T. W., and Laksmi, K.: Machine vision detection parameters for plant species identification. In: Precision agriculture and biological quality, 14, January, 1999, 3543, 327-335, <https://doi.org/10.1117/12.336896>, 1999

595 Mohapatra, J., Singh, C. P., Tripathi, O. P., and Pandya, H. A.: Remote sensing of alpine treeline ecotone dynamics and phenology in Arunachal Pradesh Himalaya. *Int. J. Remote Sens.*, 40(20), 7986-8009, <https://doi.org/10.1080/01431161.2019.1608383>, 2019.

Richardson, A. J., and Wiegand, C. L.: Distinguishing vegetation from soil background information. *Photogramm. Eng. Remote Sens.*, 43(12), 1541-1552, 1977.

Ronneberger, O., Fischer, P., and Brox, T.: U-net: Convolutional networks for biomedical image segmentation, in: *Medical image computing and computer-assisted intervention–MICCAI 2015: 18th international conference, Munich, Germany, 5-9, October, 2015, proceedings, part III 18*. Springer international publishing, edited by: Navab, N., Hornegger, J., Wells, W., Frangi, A., Springer, Cham, 234-241, [https://doi.org/10.1007/978-3-319-24574-4\\_28](https://doi.org/10.1007/978-3-319-24574-4_28), 2015.

Rösch, M., Sonnenschein, R., Buchelt, S., and Ullmann, T.: Comparing PlanetScope and Sentinel-2 imagery for mapping mountain pines in the Sarntal Alps, Italy. *Remote Sens.*, 14(13), 3190, <https://doi.org/10.3390/rs14133190>, 2022.

Rouse Jr, J. W., Haas, R. H., Schell, J. A., and Deering, D. W.: Monitoring vegetation systems in the Great Plains with ERTS, in *Proceedings of the 3rd ERTS Symposium*, Washington, DC, USA, 1, 309-317, 1974

Rubner, Y., Puzicha, J., Tomasi, C., and Buhmann, J. M.: Empirical evaluation of dissimilarity measures for color and texture. *Comput. Vis. Image Underst.*, 84(1), 25-43, <https://doi.org/10.1006/cviu.2001.0934>, 2001.

Rumpf, S. B., Gravey, M., Brönnimann, O., Luoto, M., Cianfrani, C., Mariethoz, G., and Guisan, A.: From white to green: Snow cover loss and increased vegetation productivity in the European Alps. *Science*, 376(6597), 1119-1122, <https://doi.org/10.1126/science.abn6697>, 2022.

Sibuya, B., Lottering, R., and Odindi, J.: Discriminating commercial forest species using image texture computed from a worldview-2 pan-sharpened image and partial least squares discriminant analysis. *Remote Sens. Appl.: Soc. Environ.*, 23, 100605, <https://doi.org/10.1016/j.rsase.2021.100605>, 2021.

Sonnentag, O., Hufkens, K., Teshera-Sterne, C., Young, A. M., Friedl, M., Braswell, B. H., Milliman, T., O'Keefe, J., and Richardson, A. D.: Digital repeat photography for phenological research in forest ecosystems. *Agric. For. Meteorol.*, 152, 159-177, <https://doi.org/10.1016/j.agrformet.2011.09.009>, 2012.

Terskaia, A., Dial, R. J., and Sullivan, P. F.: Pathways of tundra encroachment by trees and tall shrubs in the western Brooks Range of Alaska. *Ecography*, 43(5), 769-778, <https://doi.org/10.1111/ecog.05015>, 2020.

Wagner, F. H., Sanchez, A., Tarabalka, Y., Lotte, R. G., Ferreira, M. P., Aidar, M. P. M., Gloor, E., Phillips, O. L., and Aragão, L. E. O. C.: Using the U-net convolutional network to map forest types and disturbance in the Atlantic rainforest with very high resolution images. *Remote Sens. Ecol. Conserv.*, 5(4), 360-375, <https://doi.org/10.1002/rse2.111>, 2019.

Wang, H., Zhao, Y., Pu, R., and Zhang, Z.: Mapping *Robinia pseudoacacia* forest health conditions by using combined spectral, spatial, and textural information extracted from IKONOS imagery and random forest classifier. *Remote Sens.*, 7(7), 9020-9044, <https://doi.org/10.3390/rs70709020>, 2015.

Wang, W., Liao, M. C., and Tzeng, H. Y.: Competition in *Abies kawakamii* forests at subtropical high mountain in Taiwan. *PLoS ONE*, 16(7), e0254791, <https://doi.org/10.1371/journal.pone.0254791>, 2021.

Wang, X., Wang, T., Xu, J., Shen, Z., Yang, Y., Chen, A., Wang, S., Liang, E., and Piao, S.: Enhanced habitat loss of the Himalayan endemic flora driven by warming-forced upslope tree expansion. *Nat. Ecol. Evol.*, 6(7), 890-899, <https://doi.org/10.1038/s41559-022-01774-3>, 2022.

635 Wang, Y., Pederson, N., Ellison, A. M., Buckley, H. L., Case, B. S., Liang, E., and Julio Camarero, J.: Increased stem density and competition may diminish the positive effects of warming at alpine treeline. Ecol., 97(7), 1668-1679, https://doi.org/10.1890/15-1264.1, 2016.

Woebbecke, D. M., Meyer, G. E., Von Bargen, K., and Mortensen, D. A.: Color indices for weed identification under various soil, residue, and lighting conditions. Transactions of the ASAE, 38(1), 259-269, https://doi.org/10.13031/2013.27838, 1995

640 Xu, D., Geng, Q., Jin, C., Xu, Z., and Xu, X.: Tree line identification and dynamics under climate change in Wuyishan National Park based on Landsat images. Remote Sens., 12(18), 2890, https://doi.org/10.3390/rs12182890, 2020.

Yuan, X., King, D., and Vlcek, J.: Sugar maple decline assessment based on spectral and textural analysis of multispectral aerial videography. Remote Sens. Environ., 37(1), 47-54, https://doi.org/10.1016/0034-4257(91)90049-C, 1991.

645 Zheng, Z., Zhu, W., and Zhang, Y.: Seasonally and spatially varied controls of climatic factors on net primary productivity in alpine grasslands on the Tibetan Plateau. Glob. Ecol. Conserv., 21, e00814, https://doi.org/10.1016/j.gecco.2019.e00814, 2020.

Abutaleb, K., Newete, S. W., Manganya, S., Adam, E., and Byrne, M. J.: Mapping eucalypts trees using high resolution multispectral images: A study comparing WorldView 2 vs. SPOT 7. Egypt. J. Remote Sens. Space Sci., 24(3), 333-342, https://doi.org/10.1016/j.ejrs.2020.09.001, 2021.